

SCIENTIFIC REPORTS



OPEN

Magnetic-field induced rotation of magnetosome chains in silicified magnetotactic bacteria

Marine Blondeau^{1,2,3}, Yohan Guyodo², François Guyot², Christophe Gatel⁴, Nicolas Menguy², Imène Chebbi⁵, Bernard Haye¹, Mickaël Durand-Dubief^{5,6}, Edouard Alphandery⁵, Roberta Brayner³ & Thibaud Coradin¹ 

Received: 15 December 2017

Accepted: 19 April 2018

Published online: 16 May 2018

Understanding the biological processes enabling magnetotactic bacteria to maintain oriented chains of magnetic iron-bearing nanoparticles called magnetosomes is a major challenge. The study aimed to constrain the role of an external applied magnetic field on the alignment of magnetosome chains in *Magnetospirillum magneticum* AMB-1 magnetotactic bacteria immobilized within a hydrated silica matrix. A deviation of the chain orientation was evidenced, without significant impact on cell viability, which was preserved after the field was turned-off. Transmission electron microscopy showed that the crystallographic orientation of the nanoparticles within the chains were preserved. Off-axis electron holography evidenced that the change in magnetosome orientation was accompanied by a shift from parallel to anti-parallel interactions between individual nanocrystals. The field-induced deconstruction of the chain occurs according to two possible mechanisms: (i) each magnetosome responds individually and reorients in the magnetic field direction and/or (ii) short magnetosome chains deviate in the magnetic field direction. This work enlightens the strong dynamic character of the magnetosome assembly and widens the potentialities of magnetotactic bacteria in bionanotechnology.

Since their discovery more than 30 years ago, magnetotactic bacteria have received much attention in the fields of geological, chemical, physical and biological sciences^{1–5}. However, the processes by which they synthesize iron oxide (or sulphide) magnetic nanoparticles and organize them into chains allowing the cell to orient itself along the geomagnetic field are still far from being fully understood^{6–10}. It is well-admitted that production of the nanocrystals occurs in specialized organelles, called magnetosomes, formed by a membrane invagination at multiple sites in the cell. However, identifying the proteins controlling nucleation, size, shape and arrangement in chains of the nanocrystals, as well as the mechanisms of action of these proteins, remains a challenging task^{11–15}.

Phenotypic divergences between different species were evidenced¹⁶. In some *Magnetospirillum* sp. strains, the chain is stabilized along the longitudinal axis of the cell by an organic filament, MamK protein, while the connection of magnetosomes to this structure is provided by a protein MamJ^{17,18}. The deletion of *MamK* gene in *Magnetospirillum gryphiswaldense* MSR-1 leads to short chains separated by gaps devoid of magnetosomes, while the deletion of *MamJ* induces aggregation of magnetosomes within the cell with observable filaments not attached to the biogenic particles^{19,20}. In *Magnetospirillum magneticum* AMB-1, additional MamJ-like and MamK-like proteins were identified that are involved in the dynamic of the filament and the magnetosome organization in chain^{21–23}.

The capacity of the magnetosome chain to act as a compass is not only related to the spatial arrangement of nanocrystals, but also to their crystallographic and magnetic alignment. In some magnetotactic bacteria (e.g., *Magnetospirillum* sp.), the biogenic magnetite nanoparticles have a cubo-octahedral morphology with a magnetic

¹Sorbonne Université, CNRS, Collège de France, Laboratoire de Chimie de la Matière Condensée de Paris, 4 Place Jussieu, 75252, Paris, Cedex 05, France. ²Sorbonne Université, Museum National d'Histoire Naturelle, CNRS, Institut de Recherche pour le Développement, Institut de Minéralogie, de Physique des Matériaux et de Cosmochimie, 75252, Paris, Cedex 05, France. ³Interfaces, Traitements, Organisation et Dynamique des Systèmes (ITODYS), CNRS-UMR 7086, Université Paris 7 Denis Diderot, 15 rue Jean de Baïf, 75205, Paris, cedex 13, France. ⁴Centre d'Élaboration de Matériaux et d'Études Structurales (CEMES), CNRS-UPR 8011, Université de Toulouse, 29 rue Jeanne Marvig, 31055, Toulouse, France. ⁵Nanobactérie, Campus de l'Université d'Orsay, Batiment 201 rue Henri Becquerel, 91440, Bures-sur-Yvette, France. ⁶Department of Biosciences and Nutrition, Karolinska Institutet, SE-141 83, Hudding, Sweden. Correspondence and requests for materials should be addressed to T.C. (email: thibaud.coradin@upmc.fr)

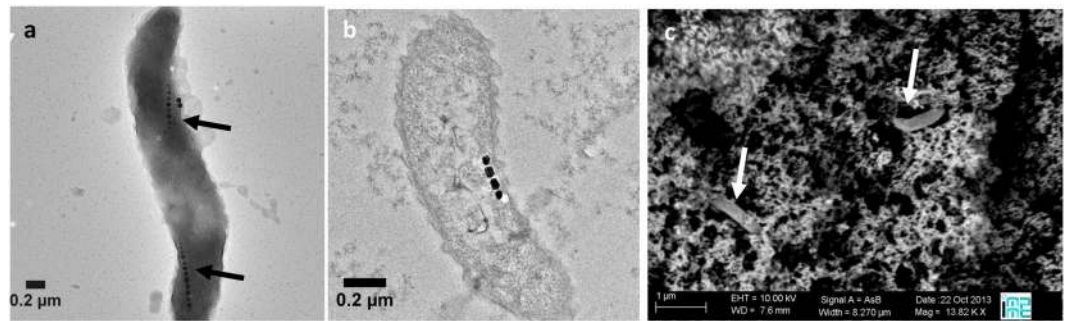


Figure 1. Electron microscopy imaging of free and silica-encapsulated magnetotactic bacteria. (a) TEM observation of *M. magneticum* AMB-1 in the initial bacterial suspension (magnetosome chains are indicated by black arrows). Bacteria encapsulated in silica gel observed by (b) TEM after ultrasectionning and (c) SEM using backscattered electrons after 1 day of encapsulation (bacteria are indicated by white arrows in silica gel).

easy axis [111] aligned along the chain axis^{24,25}. The magnetization of a given single domain crystal is also oriented parallel with respect to the others in the chain thus forming a larger-scale magnetic dipole²⁶. It could be expected that an external magnetic field present during the formation of magnetosomes, or once the chains are formed, could affect the organization of these biogenic structures. Few reports are available on the effect of an external magnetic field on the biomineralization process itself^{27–30}. The interactions between already-formed magnetosomes and an external magnetic field have been so far mainly studied on free-moving bacteria^{1,31,32} or cell-extracted magnetosomes³³. In one report, magnetotactic bacteria were immobilized in agarose gels, allowing for the observation a field-induced re-orientation of the chains without rotation of the whole bacterial cell³⁴. Importantly the chain deviation was shown to be reversible when the field was turned off, suggesting that the assembly of proteins involved in the nanocrystal organization had a dynamic character.

These intriguing observations opened many additional questions such as the effect of chain re-orientation on cell viability as well as its impact on the crystallographic and magnetic orientation of the nanoparticles. Aiming to go further in the understanding of these processes, we have used here a mineral matrix, made of hydrated silica, as an encapsulation host for the AMB-1 magnetotactic bacteria, in order to prevent their motility in presence of an external magnetic field. This mineral matrix can be obtained in water, near neutral pH and at room temperature³⁵. It is transparent, chemically-stable and not biodegradable by most living organisms. Such cellular hosts have been previously shown to be compatible with the long-term viability of several strains of bacteria and many other living cells³⁶. In these environments, bacteria are confined in a cavity adapted to their size, preventing their motility, and cell division is hindered to insure that the population remains constant over the whole experiment³⁷.

In these conditions, it was possible to observe the stable reorientation of magnetosome chains within living magnetotactic bacteria exposed to an external magnetic field. The detailed study of the resulting crystallographic and magnetic structures pointed out the dynamic character of the protein set involved in the organization of the magnetosome chains.

Results

Bacterial encapsulation and viability. Initially, AMB-1 cells were cultivated in presence of 20 μM of ferric quinate allowing for the production of magnetosomes. According to the transmission electron microscopy (TEM) observations, these bacteria had as expected biogenic nanoparticles aligned into one or more chains (Fig. 1a). After one day of encapsulation of a bacterial suspension (in phosphate buffer 10 wt% glycerol) in an aqueous silica gel, the ultrastructure of the bacteria remained well preserved (Fig. 1b) and scanning electron microscopy (SEM) images showed that the cells were well dispersed in the porous mineral network (Fig. 1c). Within the encapsulated bacterium in Fig. 1b, magnetosomes with a size typical of 40–50 nm were aligned in chain located on average at 34 nm away from the cytoplasmic membrane. The distance between individual nanoparticles was *ca.* 7 nm. These values were typical of this type of cells, suggesting that the encapsulation process did not impact magnetosome organization^{11,12}.

In order to evaluate the viability of the magnetotactic bacteria encapsulated in gels, a colorimetric Alamar Blue test was used to directly quantify the whole viable cells comprising also non-cultivable bacteria. This test allows for the monitoring of the oxygen-consuming metabolism of the cells and was shown to fully correlate with the plate count technique for bacterial viability quantification in the case of silica-encapsulated bacteria³⁸. The Alamar Blue test indicated that after 7 days of encapsulation, 28% (+/–4%) of bacteria were alive in gels (Fig. S1). In parallel, the bacterial gels were exposed to an external static magnetic field of 80 mT by means of two parallel magnets placed on either side of flasks containing cells (Fig. S2). A nearly identical viability rate of 27% (+/–4%) was obtained after 7 days, indicating that the magnetic field did not significantly affect the viability of the bacteria over this period (Fig. S1).

Magnetic properties of bacteria encapsulated in silica gel. Direct current (DC) induced magnetizations and backfield demagnetizations of the bacteria encapsulated in silica aerogel after 1 day were acquired at room temperature. The hysteresis loop displayed a magnetic behavior typical of a mixture between diamagnetic (negative slope of the curve, noticeable at high fields) and ferro- or ferri-magnetic (open hysteresis) materials

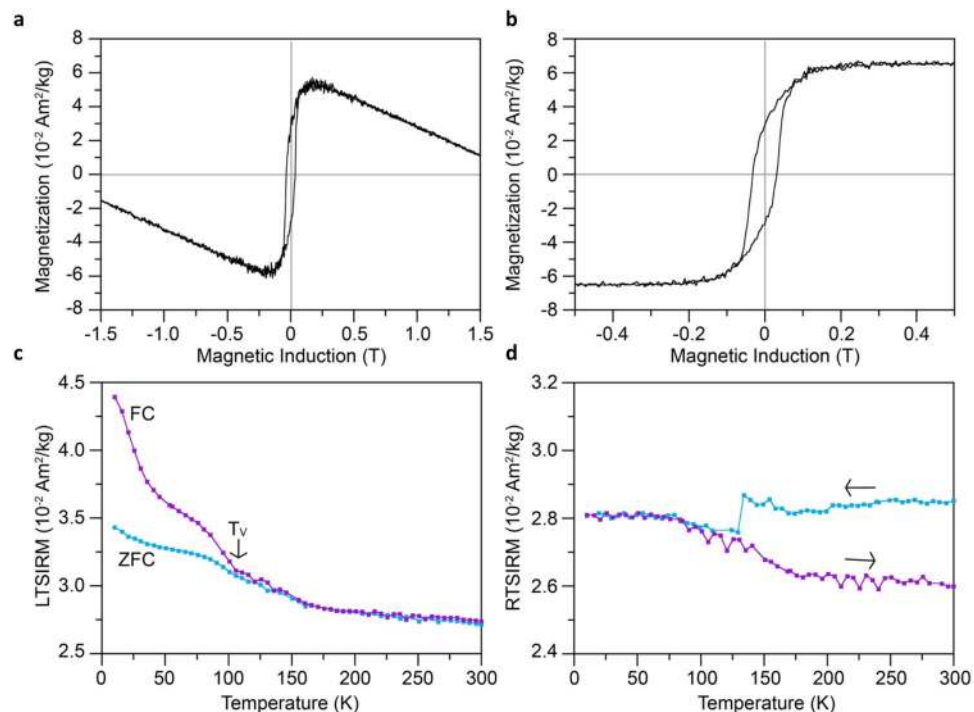


Figure 2. Magnetic properties of silica-encapsulated magnetotactic bacteria. Magnetization curves for the AMB-1 cell-containing aerogel after 1 day acquired at 300 K (a) between -1.5 T and $+1.5$ T and (b) between -0.5 T and $+0.5$ T with correction of the diamagnetic component. (c) Field Cooling (FC) and Zero Field Cooling (ZFC) thermal demagnetization curves of the low-temperature saturation isothermal remanent magnetization (LT-SIRM) acquired at 10 K in a 2.5 T induction for the AMB-1 bacterial aerogel after 1 day. (d) Cooling (in blue) and warming (in purple) curves of the room-temperature saturation isothermal remanent magnetization (RT-SIRM) acquired at 300 K in a 2.5 T magnetic induction.

(Fig. 2a). Mathematical subtraction of the diamagnetic contribution allowed us to isolate the ferrimagnetic contribution of the nanocrystals (Fig. 2b). The sample was characterized by saturation magnetization (M_s) and saturation remanent magnetization (M_{rs}) values of 0.065 and 0.030 $\text{Am}^2\cdot\text{kg}^{-1}$, respectively. The saturation magnetization was very low due to the dispersion of the cells within the silica matrix. The sample coercivity (B_c) and coercivity of remanence (B_{cr}) obtained from backfield measurements were 32 and 38 mT, respectively. The B_{cr}/B_c and M_{rs}/M_s ratios were 1.19 and 0.46 , respectively. These values are close to those previously reported for whole cell AMB-1^{39–42}.

Thermal demagnetization curves of low-temperature saturation remanent magnetization (acquired in 2.5 T at 10 K) after cooling from room temperature in zero magnetic field (zero field cooling, ZFC) or in a 2.5 T magnetic induction (field cooling, FC) displayed a drop in magnetization around 100–110 K characteristic of the Verwey transition, in agreement with previous other AMB-1 samples³⁹ (Fig. 2c). The Verwey transition was also clearly visible on the cooling and warming curves of the room temperature (acquired at 300 K in 2.5 T), attesting that bacterial nanocrystals corresponded to magnetite (Fig. 2d)⁴³. In addition, the rather flat aspect of the cooling curve above the transition indicated that our samples were not oxidized. δ_{FC} and δ_{ZFC} ratios⁴¹ were equal to 0.14 and 0.09 , respectively. The δ_{FC}/δ_{ZFC} ratio of 1.5 was below the commonly accepted cut-off value of 2 for intact chains of magnetosomes. This suggests that: (i) some chains were disrupted during the CO_2 supercritical drying for aerogel preparation or (ii) bacteria were encapsulated at different stages of magnetosome chains formation^{39,41,44}.

Effect of the magnetic field on magnetosome orientation. The bacteria entrapped in silica matrix without further iron supply (to limit the production of new magnetosomes) were observed after 7 days of exposition or not to an external magnetic field of up to 80 mT (Fig. 3). Whereas the orientation of the magnetosome chains parallel to the bacterial longitudinal axis was preserved in the absence of magnetic field (Fig. 3a), some of the bacteria exposed to the 80 mT field presented several chains of magnetosomes disposed parallel between them but inclined relative to the longitudinal axis of the bacteria (Fig. 3b). Noticeably, those two orientations were sometimes observed within one cell (Fig. 3c). The length of magnetosomes chains oriented transversely to the cell body varied from one bacterium to another (chains of 3 to 6 nanocrystals) (Figs 3b,c and S3). Importantly, bacteria in suspension after 7 days in presence of a magnetic field presented the same magnetosome orientations as in the initial bacterial suspension, indicating that these unusual chain orientations were due to the combination of cell immobilization and external magnetic field.

Further information was obtained using off-axis Electron Holography (EH), a powerful interferometric TEM method to correlate morphological microscopy information and local magnetic measurements of nanomaterials^{45–49}. This technique allows a quantitative mapping of the magnetic properties of magnetosome chains at

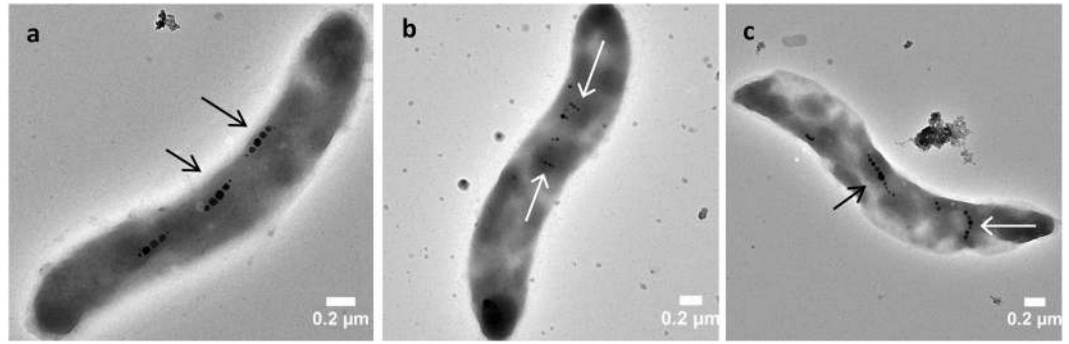


Figure 3. TEM images of silica-encapsulated magnetotactic bacteria exposed, or not, to an external magnetic field. AMB-1 cells kept in (a) absence or (b,c) presence of an 80 mT magnetic field during 7 days of encapsulation. (Black arrows show undeviated chains and white arrows show deviated chains).

the nanoscale^{26,50–54}. Here, bacteria with pre-existing magnetosomes in suspension and unexposed to the external magnetic field were first observed after 7 days (Fig. 4a). The contour map of the magnetic flux inside and outside the magnetosome chains suggests that the biogenic particles were coupled parallel and that the magnetization of each magnetosome was aligned forming a magnetic dipole as usually observed in magnetotactic bacteria²⁶ (Fig. 4b,c). Encapsulated bacteria were observed after 7 days of exposure to a magnetic field (Fig. 4d,g). In bacterium containing only chains deviated off the cell longitudinal axis (Fig. 4d), off-axis EH images displayed anti-parallel coupling between the magnetosomes (Fig. 4e) whereas for bacterium exhibiting both parallel and deviated chains off the cell longitudinal axis (Fig. 4g), two magnetic configurations were observed: (i) an anti-parallel coupling in deviated chain (Fig. 4h) and (ii) a parallel coupling in parallel chain (Fig. S4).

Complementary experiments were performed to determine how the magnetosomes re-oriented in the applied magnetic field. High-resolution TEM (HRTEM) analyses were used to determine the crystallographic axes in nanoparticles from different chains previously studied by electron holography. In the magnetosome chain of the bacterium not exposed to the magnetic field, the [111] axes were aligned parallel to the bacterial longitudinal axis (Figs 4c and S5), as already observed for *Magnetospirillum* sp.^{24,26}. The same crystallographic orientation was observed for the bacterium containing only chains deviated off the longitudinal cell axis (Figs 4f and S6) and for the bacterium where both chain orientations coexisted (Figs 4i and S7). Some [111] axes in deviated chains in both bacteria (Fig. 4f,i) were oriented in the direction or close to the direction of the particles magnetization (Fig. 4e,h). In the chain placed along the longitudinal axis of the cell (Figs 4g, S4 and S8), the [111] axes of magnetosomes preserved their orientations parallel to the magnetization and in the chain direction.

Discussion

So far, the influence of a magnetic field on magnetosome within magnetotactic bacteria has been mainly studied on cell suspensions, showing noticeable effects on magnetosome size, morphology and rate of production^{27–30}. One study by Körnig *et al.* reported the effect of a magnetic field on MSR-1 bacteria entrapped within an agarose hydrogel³⁴. At sufficiently high magnetic field (35 mT and above), a rotation of the nanocrystals to align along the field direction was reported. When these cells were fixed with paraformaldehyde (i.e. preserving the intracellular organization when the field is turned off), short chains were observed that were also aligned along the field direction. Such a disruption of the chain organization was further evidenced by application of a second field that could re-orientate the chains only if the first field had an intensity above 35 mT. Interestingly, if the first field was turned off without cell chemical fixation, the initial chains were recovered. Such reversibility would suggest that the assembly of MamK/MamJ proteins responsible for chain integrity had a strong dynamic character, allowing for chain reconstruction after the field-induced disruption.

Compared to this previous study, our system has several specificities. First it must be pointed out that the magnetotactic bacteria strain we used, AMB-1, does not show the exact same set of proteins as MSR-1^{16–23}, which could at least explain some of the differences between the two systems. Contrary to some magnetotactic bacteria which are difficult to isolate, cultivate⁵⁵ or are obligate microaerophile^{56,57}, AMB-1 bacteria grow in liquid culture medium and on agar plates in presence of oxygen⁵⁸. This strain is not obligate microaerophile and can therefore be easily manipulated for various applications^{2,59,60}. The incubation of these oxygen-tolerant bacteria in culture medium bottle without stirring and air exchange at 30 °C permitted to obtain microaerophilic conditions favoring the magnetosomes productions. In our experiments, the oxygen tolerance of AMB-1 bacteria limited the stress of the encapsulation in an air atmosphere. Compared to *M. gryphiswaldense*, *M. magneticum* possess additional proteins (MamK-like and MamJ-like) acting in the chain magnetosomes organization and dynamic of the filament^{21,23}. Consequently, the cell response to a magnetic environment may depend on the strain and phenotypic divergences⁶¹. Second, whereas in the previous study, the MSR-1 cells were initially aligned by a magnetic field before their immobilization in agarose, the AMB-1 cells were here more randomly distributed within the silica gel when it formed and trapped the bacteria. In other words, if the observed magnetosome and/or chain orientation was strictly reflecting the external field direction, all organizations within a single bacterium should be the same, in contradiction with our observations. Finally, and more importantly, the chains deviated off the longitudinal cell axis were here observed when the external magnetic field was turned-off without the need for cell fixation. This calls for the examination of alternative mechanisms.

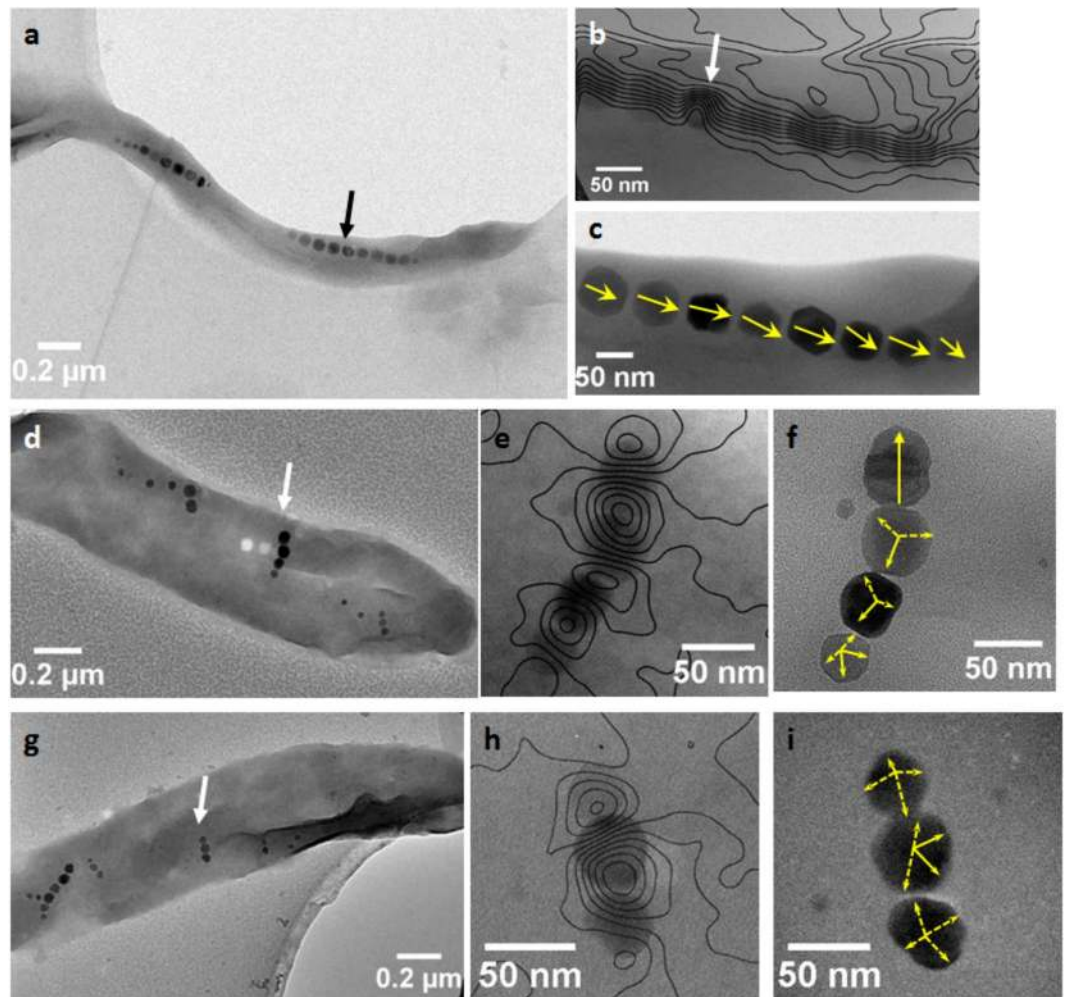


Figure 4. Electron microscopy observations of magnetic and crystallographic orientations in magnetosomes. (a) TEM image of an AMB-1 cell in suspension observed after 7 days of incubation in absence of a magnetic field (black arrow shows the selected chain for off-axis image), (b) corresponding magnetic phase contours of magnetosome chains determined by off-axis EH (d,g) TEM images of encapsulated AMB-1 bacteria observed after 7 days of incubation in presence of a magnetic field (white arrows show the selected chains for off-axis images), (e,h) corresponding magnetic phase contours of magnetosomes chains determined by off-axis EH and (c,f,i) corresponding HRTEM images with $\langle 111 \rangle$ directions determined by using Selected Area Electron Diffraction (SAED) and materialized by yellow bars.

It seems crucial to first consider magnetosome nanocrystals and chains of magnetosomes independently. Electron microscopy studies on bacteria-containing gels after 1 and 7 days in the absence of external field indicated that the intracellular content of the initial magnetotactic bacteria was well-preserved within the silica network. In this situation, single domain magnetite nanoparticles were arranged in chains oriented parallel to the longitudinal axis of the cell. When the magnetic field was applied on the encapsulated bacteria, we observed that (i) some chains were no longer parallel to the cell longitudinal axis and remained so even if the field is turned-off, (ii) in these chains, the magnetosomes interacted via an anti-parallel magnetic coupling, (iii) they preserved their relative crystallographic co-alignment, (iv) these modifications did not seem to have a significant detrimental effect on cell viability (as compared to encapsulated cells aged without external field).

Some studies of *M. gryphiswaldense* MSR-1, have suggested that the magnetosome vesicles form a distinct compartment detached from the cytoplasmic membrane¹⁷. The nucleation of magnetite crystals would take place in invagination of the cytoplasmic membrane, favoring iron transfer from the external medium; the vesicles would then detach at some stage of the biomineralization process^{62,63}. A dynamic filamentous protein MamK would play a role in the maintenance of chain continuity by reducing gaps between magnetosomes in *M. magneticum* AMB-1^{18,64}. Note that some remaining contact between the magnetic chain and the membrane is necessary to permit the alignment of the cell in the geomagnetic field³. From this starting situation (Fig. 5a), the effect of the magnetic field can occur according to two hypothetical mechanisms:

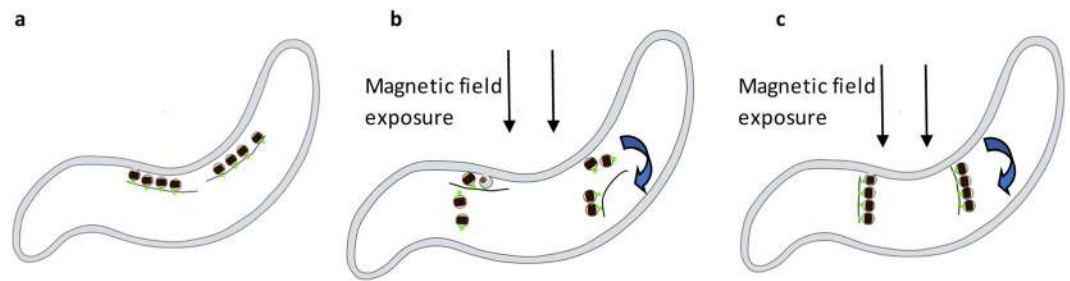


Figure 5. Schematic representation of the possible mechanisms involved in deviated magnetosome chains. (a) AMB-1 bacteria with magnetosome chains connected to the cytoplasmic membrane via an invagination and stabilized by the molecular complex MamK/MamJ. (b) Magnetosome chains disrupted during the magnetic field exposition. Each magnetosome responds individually to the field and arranges again in chain thanks to the molecular complex MamK/MamJ. (c) Whole magnetosome chains as one entity orient directly in the magnetic field direction.

- (i) The integrity of the whole chain is lost, allowing for the motion of individual magnetosomes in the magnetic field, that could be then collected and reassembled by the dynamic structural proteins MamK and MamJ (Fig. 5b). It has been suggested that the formation of magnetosome chains was a step-by-step process in which each particle is synthesized consecutively so that the orientation of the growing one is imposed by those already present^{6,33,65,66}. Here, as each magnetite nanocrystal would respond individually to the magnetic field before being reassembled, their relative crystallographic and magnetic orientation is difficult to predict.
- (ii) The structures connecting magnetosomes to the cytoplasmic membrane would be disrupted to the exception of some possible anchoring sites and the protein filament insuring the chain integrity would be preserved. Then the whole chain would turn to align its global magnetic dipole along the external field (Fig. 5c). In this situation the crystalline orientation of the magnetosomes should be preserved whereas modification in the magnetic interactions can occur.

Here, we found out that the crystalline orientation within deviated chains after the field is turned off can be similar to non-deviated chains (i.e. [111] axis parallel to the chain direction). It is important to point out that compared to Körnig *et al.*³⁴, the cells were still alive (not chemically fixed) when the field was turned-off so that they could preserve their ability to synthesize the proteins involved in chains organization, orientation and interaction with the inner membrane. Turning to magnetic interactions, anti-parallel coupling has been observed in deviated chains of magnetosomes whereas parallel coupling was present in non-deviated ones. Overall, the magnetic field exposure has favored the deconstruction of magnetosome chains organization.

In conclusion, our results shade new light on the mechanisms by which magnetotactic bacteria are able to control the assembly of magnetic nanocrystals within magnetosome chains. Our observation of a stable deviation of the chain orientation within living cells suggests that the assembly of cytoskeletal proteins regulating the nanocrystal organization would have a significant dynamic character, echoing recent evidences of the role of actin in iron oxide biomineralization in honeybees⁶⁷. Some other proteins could also have a role in maintaining stable deviated chains by interacting with magnetosomes and the cytoplasmic membrane. Of significance for the field of magnetotactic bacteria is the fact that the underlying process, and therefore the associated set of proteins, may be specific to AMB-1, providing an additional evidence of phenotypic divergence in this group of biomineralizing bacteria. The here-demonstrated possibility to manipulate chain orientation without impacting cell viability may also open opportunities for the use of encapsulated magnetotactic bacteria within functional devices.

Methods

Bacteria culture. *Magnetospirillum magneticum* strain AMB-1 ATCC 700264 was grown in culture medium containing KH_2PO_4 (0.68 g/L), Succinic acid (0.37 g/L), Tartaric acid (0.37 g/L), Sodium acetate (0.05 g/L), NaNO_3 (0.12 g/L), Ascorbic acid (0.035 g/L), *Wolfe's Vitamin Solution* (10 mL), *Wolfe's Mineral Solution* (5 mL), and ferric quinate (0.01 M) (2 mL). *Wolfe's Vitamin Solution* (ATCC) contains Biotin (2 mg/L), Folic acid (2 mg/L), Pyridoxine (10 mg/L), Thiamine (5 mg/L), Riboflavin (5 mg/L), nicotinic acid (5 mg/L), pantothenic acid (5 mg/L), vitamin B12 (0.1 mg/L), p-Aminobenzoic acid (5 mg/L), Thiocetic acid (5 mg/L). *Wolfe's Mineral Solution* (non ATCC) contains Nitrilotriacetic acid (0.5 g/L), $\text{MgSO}_4 \cdot 7\text{H}_2\text{O}$ (1.5 g/L), $\text{MnSO}_4 \cdot \text{H}_2\text{O}$ (1 g/L), NaCl (0.5 g/L), $\text{FeSO}_4 \cdot 7\text{H}_2\text{O}$ (0.1 g/L), $\text{CoNO}_3 \cdot 6\text{H}_2\text{O}$ (0.1 g/L), CaCl_2 (0.1 g/L), $\text{ZnSO}_4 \cdot 7\text{H}_2\text{O}$ (0.1 g/L), $\text{CuSO}_4 \cdot 5\text{H}_2\text{O}$ (0.01 g/L), $\text{AlK}(\text{SO}_4)_2 \cdot 12\text{H}_2\text{O}$ (0.01 g/L), H_3BO_3 (0.01 g/L), Na_2MoO_4 (0.01 g/L), Na_2SeO_3 (0.002 g/L), EDTA (0.5 g/L). The pH of the medium was adjusted to 6.75 with sodium hydroxide solution (1 M) and sterilized.

1.8 mL of AMB-1 strain culture, stored at -80°C , are inoculated in a flask of 20 mL with 15 mL of culture medium containing ferric quinate (20 μM). The bacteria preculture is incubated at 30°C for 4 to 10 days. 10 mL of preculture are then added in a bottle of 1 L containing 1 L of iron-rich culture medium (20 μM of ferric quinate) to permit the production of magnetosomes. The incubation is performed over 7 days at 30°C .

Bacteria encapsulation. The culture with magnetosomes was centrifuged at $6000 \times g$ during 30 minutes at 5°C , then the pellet was suspended with 4 mL of phosphate buffer (pH 7.2) containing 10 wt% glycerol. The

bacterial suspension was adjusted to an optical density (OD) of 5. Silica gels were prepared from a precursor of sodium silicate solution (27 wt% SiO₂, 10 wt% NaOH) from Sigma Aldrich. A mixture of sodium silicate (0.8 M, 1 mL) and glycerol (10 wt%, 1 mL) was neutralized with hydrochloric acid (4 M, 0.155 mL) under stirring. After 5 seconds, 1 mL of bacterial suspension (OD = 5) was added and the assemblage was stirred for 5 minutes. The gels were formed after 5–6 min at room temperature and were then kept at 20 °C for up to 7 days.

The encapsulated bacteria were exposed to an external static magnetic field created by two parallel magnets. The magnets were placed in a set-up realized with Plexiglas™ and were spaced of 5 cm that permitted to have a field of 55 mT in the center of the set-up and 80 mT at each magnet (see Fig. 2b).

Characterization of bacteria-silica aerogels. In order to obtain dried material, AMB-1 containing silica gels were converted into aerogels via supercritical drying as described thereafter. Shortly, the bacterial gels are first fixed with a glutaraldehyde solution (2.5%) for 1 hour and washed 3 times in a buffer. Then the samples are dehydrated in different baths of ethanol and dried by using a CO₂ supercritical point dryer.

The aerogel magnetization was first measured as a function of the applied field magnetic intensity at 300 K using a Vibrating Sample Magnetometer (VSM) model 3900 from Princeton Measurements Corporation. Low-temperature measurements were performed using a Superconducting Quantum Interference Device (SQUID) magnetometer MPMS XL-5 from Quantum Design.

Scanning electron microscopy (SEM) was performed using a Zeiss Ultra 55 SEM-FEG microscope on a carbon-coated aerogel crushed sample.

Characterization of silica-extracted bacteria. Bacterial gels were dispersed in 5 ml of phosphate buffer, then broken with 4 mm glass beads under stirring for 15 minutes. The resuspended gels were then diluted in phosphate buffer before performed viability tests using the Alamar Blue method³⁸.

For TEM observations, the resuspended gels were centrifuged at 600 × g at 10 °C during 15 min to sediment the gel aggregates. The supernatant containing bacteria was collected and diluted in phosphate buffer. All diluted suspensions were washed by centrifugation at 6000 × g at 10 °C during 15 min. The supernatant was removed and 3 ml of the bottom were kept and homogenized. 10 μL of concentrated bacterial suspension were placed on copper grids covered with thin carbon film and dried at 30 °C during 3 hours to permit sedimentation of cells on the carbon film. Then the bacteria were fixed with 10 μL of glutaraldehyde (2.5%) for 1 hour at 4 °C. The samples were then washed with ultrapure water and dried before the observation by TEM using a JEOL TEM 2100 equipped with an LaB6 crystal gun, with an accelerating tension of 200 kV. The high-resolution TEM (HRTEM) has been performed on the same samples by using a TEM JEOL-2100F operating at 200 kV and equipped with a field emission gun (FEG). The in-plane crystallographic direction and observed zone axes have been determined by using the Fast Fourier transform on the two-dimensional HRTEM images and have permitted to deduce then the corresponding stereographic projection for each particle. Off-axis electron holography (EH) was carried out using Hitachi HF3300C microscope, following previously described protocols^{26,45,46,68,69}. Ultrathin sections of bacterial gels were prepared according to the following protocol. The bacterial gels were first fixed with a glutaraldehyde solution (2.5%) for 1 hour and washed 3 times in a buffer, then fixed with osmium tetroxide solution (2%) for 1 hour before washed 3 times in a buffer. The samples were then dehydrated in different baths of ethanol and embedded in Araldite® resin.

Data availability. No datasets were generated or analysed during the current study.

References

- Blakemore, R. P. Magnetotactic Bacteria. *Ann. Rev. Microbiol.* **36**, 217–238 (1982).
- Faivre, D. & Schüler, D. Magnetotactic bacteria and magnetosomes. *Chem. Rev.* **108**, 4875–98 (2008).
- Komeili, A. Molecular mechanisms of compartmentalization and biomineralization in magnetotactic bacteria. *FEMS Microbiol. Rev.* **36**, 232–255 (2012).
- Lefèvre, C. T. & Bazylinski, D. A. Ecology, diversity, and evolution of magnetotactic bacteria. *Microbiol. Mol. Biol. Rev.* **77**, 497–526 (2013).
- Prozorov, T., Bazylinski, D. A., Mallapragada, S. K. & Prozorov, R. Novel magnetic nanomaterials inspired by magnetotactic bacteria: Topical review. *Mater. Sci. Eng.: R: Rep.* **74**, 133–172 (2013).
- Frankel, R. B. Magnetic guidance of organisms. *Ann. Rev. Biophys. Bioeng.* **13**, 85–103 (1984).
- Frankel, R. B. & Bazylinski, D. A. How magnetotactic bacteria make magnetosomes queue up. *Trends Microbiol.* **14**, 329–331 (2006).
- Mao, X., Egli, R., Petersen, N., Hanzlik, M. & Zhao, X. Magnetotaxis and acquisition of detrital remanent magnetization by magnihetotactic bacteria in natural sediment: First experimental results and theory. *Geochem. Geophys. Geosyst.* **15**, 255–283 (2014).
- Popp, F., Armitage, J. P. & Schüler, D. Polarity of bacterial magnetotaxis is controlled by aerotaxis through a common sensory pathway. *Nat. Commun.* **5**, 5398, <https://doi.org/10.1038/ncomms6398> (2014).
- Zhu, X. *et al.* Angle sensing in magnetotaxis of *Magnetospirillum magneticum* AMB-1. *Integr. Biol. (Camb)* **6**, 706–713 (2014).
- Gorby, Y. A., Beveridge, T. J. & Blakemore, R. P. Characterization of the bacterial magnetosome membrane. *J. Bacteriol.* **170**, 834–841 (1988).
- Bazylinski, D. A. & Frankel, R. B. Magnetosome formation in prokaryotes. *Nat. Rev. Microbiol.* **2**, 217–230 (2004).
- Komeili, A., Vali, H., Beveridge, T. J. & Newman, D. K. Magnetosome vesicles are present before magnetite formation, and MamA is required for their activation. *Proc. Natl. Acad. Sci. USA* **101**, 3839–3844 (2004).
- Nudelman, H. & Zarivach, R. Structure prediction of magnetosome-associated proteins. *Front. Microbiol.* **5**, 9 (2014).
- Uebe, R. & Schüler, D. Magnetosome biogenesis in magnetotactic bacteria. *Nat. Rev. Microbiol.* **14**, 621–637 (2016).
- Richter, M. *et al.* Comparative Genome Analysis of Four Magnetotactic Bacteria Reveals a Complex Set of Group-Specific Genes Implicated in Magnetosome Biomineralization and Function. *J. Bacteriol.* **189**, 4899–4910 (2007).
- Scheffel, A. *et al.* An acidic protein aligns magnetosomes along a filamentous structure in magnetotactic bacteria. *Nature* **440**, 110–114 (2006).
- Komeili, A., Li, Z., Newman, D. K. & Jensen, G. J. Magnetosomes Are Cell Membrane Invasions Organized by the Actin-Like Protein MamK. *Science* **311**, 242–245 (2006).

19. Scheffel, A. & Schuler, D. The Acidic Repetitive Domain of the *Magnetospirillum gryphiswaldense* MamJ Protein Displays Hypervariability but Is Not Required for Magnetosome Chain Assembly. *J. Bacteriol.* **189**, 6437–6446 (2007).
20. Katzmann, E., Scheffel, A., Gruska, M., Plitzko, J. M. & Schüler, D. Loss of the actin-like protein MamK has pleiotropic effects on magnetosome formation and chain assembly in *Magnetospirillum gryphiswaldense*. *Mol. Microbiol.* **77**, 208–224 (2010).
21. Rioux, J.-B. *et al.* A Second Actin-Like MamK Protein in *Magnetospirillum magneticum* AMB-1 Encoded Outside the Genomic Magnetosome Island. *PLoS ONE* **5**, e9151 (2010).
22. Draper, O. *et al.* MamK, a bacterial actin, forms dynamic filaments *in vivo* that are regulated by the acidic proteins MamJ and LimJ. *Mol. Microbiol.* **82**, 342–354 (2011).
23. Abreu, N. *et al.* Interplay between two bacterial actin homologs, MamK and MamK-Like, is required for the alignment of magnetosome organelles in *Magnetospirillum magneticum* AMB-1. *J. Bacteriol.* **196**, 3111–3121 (2014).
24. Mann, S., Frankel, R. B. & Blakemore, R. P. Structure, morphology and crystal growth of bacterial magnetite. *Nature* **310**, 405–407 (1984).
25. Bazylinski, D. A., Garratt-Reed, A. J. & Frankel, R. B. Electron microscopic studies of magnetosomes in magnetotactic bacteria. *Microsc. Res. Tech.* **27**, 389–401 (1994).
26. Dunin-Borkowski, R. E. *et al.* Magnetic Microstructure of Magnetotactic Bacteria by Electron Holography. *Science* **282**, 1868–1870 (1998).
27. Wang, X., Liang, L., Song, T. & Wu, L. Sinusoidal magnetic field stimulates magnetosome formation and affects mamA, mms13, mms6, and magA expression in *Magnetospirillum magneticum* AMB-1. *Can. J. Microbiol.* **54**, 1016–1022 (2008).
28. Wang, X., Liang, L., Song, T. & Wu, L. Magnetosome formation and expression of mamA, mms13, mms6 and magA in *Magnetospirillum magneticum* AMB-1 exposed to pulsed magnetic field. *Curr. Microbiol.* **59**, 221–226 (2009).
29. Wang, X. & Liang, L. Effects of static magnetic field on magnetosome formation and expression of mamA, mms13, mms6 and magA in *Magnetospirillum magneticum* AMB-1. *Bioelectromagnetics* **30**, 313–321 (2009).
30. Pan, W. *et al.* Effects of pulsed magnetic field on the formation of magnetosomes in the *Magnetospirillum* sp. strain AMB-1. *Bioelectromagnetics* **31**, 246–251 (2010).
31. Érglis, K. *et al.* Dynamics of Magnetotactic Bacteria in a Rotating Magnetic Field. *Biophys. J.* **93**, 1402–1412 (2007).
32. Nadkarni, R., Barkley, S. & Fradin, C. A Comparison of Methods to Measure the Magnetic Moment of Magnetotactic Bacteria through Analysis of Their Trajectories in External Magnetic Fields. *PLoS ONE* **8**, e82064 (2013).
33. Körnig, A. *et al.* Magnetite Crystal Orientation in Magnetosome Chains. *Adv. Funct. Mater.* **24**, 3926–3932 (2014).
34. Körnig, A. *et al.* Probing the Mechanical Properties of Magnetosome Chains in Living Magnetotactic Bacteria. *Nano Lett.* **14**, 4653–4659 (2014).
35. Depagne, C., Roux, C. & Coradin, T. How to design cell-based biosensors using the sol–gel process. *Anal. Bioanal. Chem.* **400**, 965–976 (2010).
36. Blondeau, M. & Coradin, T. Living materials from sol–gel chemistry: current challenges and perspectives. *J. Mater. Chem.* **22**, 22335–22343 (2012).
37. Nassif, N. *et al.* Living bacteria in silica gels. *Nat. Mater.* **1**, 42–44 (2002).
38. Blondeau, M., Brayner, R., Guyot, F. & Coradin, T. Correlating biological methods to assess *Escherichia coli* bacteria viability in silica gels. *Anal. Methods* **6**, 2429–2431 (2014).
39. Li, J., Wu, W., Liu, Q. & Pan, Y. Magnetic anisotropy, magnetostatic interactions and identification of magnetofossils. *Geochem. Geophys. Geosyst.* **13**, Q10Z51 (2012).
40. Li, J. *et al.* A comparative study of magnetic properties between whole cells and isolated magnetosomes of *Magnetospirillum magneticum* AMB-1. *Chin. Sci. Bull.* **55**, 38–44 (2010).
41. Moskowitz, B. M., Frankel, R. B. & Bazylinski, D. A. Rock magnetic criteria for the detection of biogenic magnetite. *Earth Planet. Sci. Lett.* **120**, 283–300 (1993).
42. Pan, Y. *et al.* Rock magnetic properties of uncultured magnetotactic bacteria. *Earth Planet. Sci. Lett.* **237**, 311–325 (2005).
43. Dunlop, D. J. & Özdemir, Ö. *Rock Magnetism: Fundamentals and Frontiers*. (Cambridge University Press, 2001).
44. Carter-Stiglitz, B., Jackson, M. & Moskowitz, B. Low-temperature remanence in stable single domain magnetite. *Geophys. Res. Lett.* **29**, 33-1–33-4 (2002).
45. Dunin-Borkowski, R. E. *et al.* Off-axis electron holography of patterned magnetic nanostructures. *J. Microsc.* **200**, 187–205 (2000).
46. Dunin-Borkowski, R. E. *et al.* Off-axis electron holography of magnetic nanowires and chains, rings, and planar arrays of magnetic nanoparticles. *Microsc. Res. Tech.* **64**, 390–402 (2004).
47. Gatel, C. *et al.* Size-Specific Spin Configurations in Single Iron Nanomagnet: From Flower to Exotic Vortices. *Nano Lett.* **15**, 6952–6957 (2015).
48. Reyes, D. *et al.* Magnetic Configurations in Co/Cu Multilayered Nanowires: Evidence of Structural and Magnetic Interplay. *Nano Lett.* **16**, 1230–1236 (2016).
49. Galindo-Gonzalez, C. *et al.* Magnetic and microscopic characterization of magnetite nanoparticles adhered to clay surfaces. *Am. Min.* **94**, 1120–1129 (2009).
50. Dunin-Borkowski, R. E. *et al.* Off-axis electron holography of magnetotactic bacteria: magnetic microstructure of strains MV1 and MS1. *Eur. J. Min.* **13**, 671–684 (2001).
51. Li, J. *et al.* Crystal growth of bullet-shaped magnetite in magnetotactic bacteria of the *Nitrospirae* phylum. *J. R. Soc. Interface* **12**, <https://doi.org/10.1098/rsif.2014.1288> (2015).
52. Simpson, E. T. *et al.* Magnetic induction mapping of magnetite chains in magnetotactic bacteria at room temperature and close to the Verwey transition using electron holography. *J. Phys.: Conf. Ser.* **17**, 108–121 (2005).
53. Devouard, B. *et al.* Magnetite from magnetotactic bacteria; size distributions and twinning. *Am. Min.* **83**, 1387–1398 (1998).
54. Pósfai, M., Kasama, T. & Dunin-Borkowski, R. E. Characterization of Bacterial Magnetic Nanostructures Using High-Resolution Transmission Electron Microscopy and Off-Axis Electron Holography. in *Magnetoreception and Magnetosomes in Bacteria 197–225* (Springer, Berlin, Heidelberg, 2006).
55. Schüler, D. and Bazylinski, D. A. In *Manual of Environmental Microbiology*, 2nd ed. (Hurst, C. J. *et al.* Eds.); ASM Press: Washington, DC; p 1129 (2007).
56. Blakemore, R. P., Maratea, D. & Wolfe, R. S. Isolation and pure culture of a freshwater magnetic spirillum in chemically defined medium. *J. Bacteriol.* **140**(2), 720–729 (1979).
57. Maratea, D. & Blakemore, R. P. *Aquaspirillum magnetotacticum* sp. nov., a magnetic spirillum. *Int. J. Syst. Bacteriol.* **31**, 452–455 (1981).
58. Matsunaga, T., Sakaguchi, T. & Tadokoro, F. Magnetite formation by a magnetic bacterium capable of growing aerobically. *Appl. Microbiol. Biotechnol.* **35**, 651–655 (1991).
59. Yang, C.-D., Takeyama, H., Tanaka, T. & Matsunaga, T. Effects of growth medium composition, iron sources and atmospheric oxygen concentrations on production of luciferase-bacterial magnetic particle complex by a recombinant *Magnetospirillum magneticum* AMB-1. *Enz. Microbiol. Technol.* **29**, 13–19 (2001).
60. Matsunaga, T., Okamura, Y. & Tanaka, T. Biotechnological application of nano-scale engineered bacterial magnetic particles. *J. Mater. Chem.* **14**, 2099–2105 (2004).
61. Moisesescu, C., Ardelean, I. & Benning, L. G. The effect and role of environmental conditions on magnetosome synthesis. *Front. Microbiol.* **5**, 1–12 (2014).

62. Faivre, D., Böttger, L. H., Matzanke, B. F. & Schüler, D. Intracellular magnetite biomineralization in bacteria proceeds by a distinct pathway involving membrane-bound ferritin and an iron(II) species. *Angew. Chem. Int. Ed. Engl.* **46**, 8495–8499 (2007).
63. Raschdorf, O. *et al.* Genetic and Ultrastructural Analysis Reveals the Key Players and Initial Steps of Bacterial Magnetosome Membrane Biogenesis. *PLOS Genetics* **12**, e1006101 (2016).
64. Cornejo, E., Subramanian, P., Li, Z., Jensen, G. J. & Komeili, A. Dynamic Remodeling of the Magnetosome Membrane Is Triggered by the Initiation of Biomineralization. *mBio* **7**, e01898–15 (2016).
65. Frankel, R. B. & Blakemore, R. P. Navigational compass in magnetic bacteria. *J. Magn. Magn. Mater.* **15**, 1562–1564 (1980).
66. Schüler, D. *Magnetoreception and Magnetosomes in Bacteria*. (Springer Science & Business Media, 2006).
67. Hsu, C.-Y., Ko, F.-Y., Li, C.-W., Fann, K. & Lue, J.-T. Magnetoreception System in Honeybees (*Apis mellifera*). *PLOS ONE* **2**, e395 (2007).
68. Harada, K. *et al.* Real-time observation of vortex lattices in a superconductor by electron microscopy. *Nature* **360**, 51–53 (1992).
69. Midgley, P. A. An introduction to off-axis electron holography. *Micron* **32**, 167–184 (2001).

Acknowledgements

M.B. thanks the Région Ile-de-France for funding in the framework of C’Nano IdF. C’Nano-IdF is the nanoscience competence center of Paris Region, supported by CNRS, CEA, MESR and Région Ile-de-France. We thank Corine Illoul and Jean Michel Guigner for their help in the ultramicrotomy samples preparation and microscopy observations.

Author Contributions

T.C., F.G. and R.B. conceived the experiments; M.B. conducted the experiments; M.B., F.G., Y.G., C.G., N.M., I.C., C.I., B.H., J.-M.G., M.D. and E.A. contributed to the measurements; M.B., T.C., F.G., R.B., Y.G. and C.G. analyzed and interpreted the results and M.B., T.C. and F.G. drafted the manuscript. All authors critically revised the article and approved publication.

Additional Information

Supplementary information accompanies this paper at <https://doi.org/10.1038/s41598-018-25972-x>.

Competing Interests: The authors declare no competing interests.

Publisher’s note: Springer Nature remains neutral with regard to jurisdictional claims in published maps and institutional affiliations.



Open Access This article is licensed under a Creative Commons Attribution 4.0 International License, which permits use, sharing, adaptation, distribution and reproduction in any medium or format, as long as you give appropriate credit to the original author(s) and the source, provide a link to the Creative Commons license, and indicate if changes were made. The images or other third party material in this article are included in the article’s Creative Commons license, unless indicated otherwise in a credit line to the material. If material is not included in the article’s Creative Commons license and your intended use is not permitted by statutory regulation or exceeds the permitted use, you will need to obtain permission directly from the copyright holder. To view a copy of this license, visit <http://creativecommons.org/licenses/by/4.0/>.

© The Author(s) 2018